Regular frequency patterns in the young δ Scuti star HD 261711 observed by the CoRoT[⋆] and MOST[⋆⋆] satellites[⋆⋆⋆]

K. Zwintz[1,2,⋆⋆⋆⋆], L. Fossati[3], D. B. Guenther[4], T. Ryabchikova[5], A. Baglin[6], N. Themessl[2], T. G. Barnes[7], J. M. Matthews[8], M. Auvergne[6], D. Bohlender[9], S. Chaintreuil[6], R. Kuschnig[2], A. F. J. Moffat[10], J. F. Rowe[11], S. M. Rucinski[12], D. Sasselov[13], and W. W. Weiss[2]

1 Instituut voor Sterrenkunde, K. U. Leuven, Celestijnenlaan 200D, 3001 Leuven, Belgium
  e-mail: konstanze.zwintz@ster.kuleuven.be
2 University of Vienna, Institute of Astronomy, Türkenschanzstrasse 17, 1180 Vienna, Austria
3 Argelander-Institut für Astronomie der Universität Bonn, Auf dem Hügel 71, 53121 Bonn, Germany
4 Department of Astronomy and Physics, St. Mary's University, Halifax, NS B3H 3C3, Canada
5 Institute of Astronomy, Russian Academy of Sciences, Pyatnitskaya 48, 119017 Moscow, Russia
6 LESIA, Observatoire de Paris-Meudon, 5 place Jules Janssen, 92195 Meudon, France
7 The University of Texas at Austin, McDonald Observatory, 82 Mt. Locke Rd., McDonald Observatory, Texas 79734, USA
8 Department of Physics and Astronomy, University of British Columbia, 6224 Agricultural Road, Vancouver, BC V6T 1Z1, Canada
9 Herzberg Institute of Astrophysics, National Research Council of Canada, 5071 West Saanich Road, Victoria, BC V9E 2E7, Canada
10 Départment de Physique, Université de Montréal, CP 6128, Succ. Centre-Ville, Montréal, QC H3C 3J7, Canada
11 NASA-Ames Research Park, MS-244-30, Moffett Field, CA 94035, USA
12 Department of Astronomy & Astrophysics, University of Toronto, 50 St. George Street, Toronto, ON M5S 3H4, Canada
13 Harvard-Smithsonian Center for Astrophysics, 60 Garden Street, Cambridge, MA 02138, USA

ABSTRACT

Context. The internal structure of pre-main-sequence (PMS) stars is poorly constrained at present. This could change significantly through high-quality asteroseismological observations of a sample of such stars.
Aims. We concentrate on an asteroseismological study of HD 261711, a rather hot δ Scuti-type pulsating member of the young open cluster NGC 2264 located at the blue border of the instability region. HD 261711 was discovered to be a PMS δ Scuti star using the time series photometry obtained by the MOST satellite in 2006.
Methods. High-precision, time-series photometry of HD 261711 was obtained by the MOST and CoRoT satellites in four separate new observing runs that are put into context with the star's fundamental atmospheric parameters obtained from spectroscopy. Frequency Analysis was performed using Period04. The spectral analysis was performed using equivalent widths and spectral synthesis.
Results. With the new MOST data set from 2011/12 and the two CoRoT light curves from 2008 and 2011/12, the δ Scuti variability was confirmed and regular groups of frequencies were discovered. The two pulsation frequencies identified in the data from the first MOST observing run in 2006 are confirmed and 23 new δ Scuti-type frequencies were discovered using the CoRoT data. Weighted average frequencies for each group were determined and are related to $l = 0$ and $l = 1$ p-modes. Evidence for amplitude modulation of the frequencies in two groups is seen. The effective temperature ($T_{\rm eff}$) was derived to be 8600 ± 200 K, $\log g$ is 4.1 ± 0.2, and the projected rotational velocity ($v \sin i$) is 53 ± 1 km s^{-1}. Using our $T_{\rm eff}$ value and the radius of 1.8 ± 0.5 $R_\odot$ derived from spectral energy distribution (SED) fitting, we get a luminosity $\log L/L_\odot$ of 1.20 ± 0.14 which agrees well to the seismologically determined values of 1.65 $R_\odot$ and, hence, a $\log L/L_\odot$ of 1.13. The radial velocity of 14 ± 2 km s^{-1} we derived for HD 261711, confirms the star's membership to NGC 2264.
Conclusions. Our asteroseismic models suggest that HD 261711 is a δ Scuti-type star close to the zero-age main sequence (ZAMS) with a mass of 1.8 to 1.9 $M_\odot$. With an age of about 10 million years derived from asteroseismology, the star is either a young ZAMS star or a late PMS star just before the onset of hydrogen-core burning. The observed splittings about the $l = 0$ and 1 parent modes may be an artifact of the Fourier derived spectrum of frequencies with varying amplitudes.

Key words. stars: variables: delta Scuti – stars: oscillations – stars: individual: HD 261711 – techniques: photometric – techniques: spectroscopic

1. Introduction

Asteroseismology is an important science goal in the two space missions, MOST (Walker et al. 2003) and CoRoT (Baglin 2006). Numerous publications on different asteroseismic targets reflect the importance of observations conducted with these two space telescopes. Pulsating pre-main-sequence (PMS) stars have been successfully studied with both satellites as well (e.g. Zwintz et al. 2011a). The young open cluster NGC 2264, which is rich in young stellar objects, is located in a region accessible to both telescopes and, indeed, the cluster has been observed twice by MOST and twice by CoRoT. Among the common targets of the two satellites in NGC 2264 is the young δ Scuti star HD 261711, the subject of this study.

NGC 2264 ($\alpha_{2000} = 6^{\rm h} 41^{\rm m}$, $\delta_{2000} = +9° 53'$) was studied frequently in the past using various instruments in different wavelength ranges from space and from the ground. The cluster is located in the Monoceros OB1 association about 30 pc above the galactic plane and has a diameter of ~39 arcmin. Sung et al. (1997) report a cluster distance of 759 ± 83 pc which corresponds to a distance modulus of 9.40 ± 0.25 mag. Kharchenko et al. (2001) find proper motion values of -2.70 ± 0.25 mas/yr in right ascension and -3.50 ± 0.26 mas/yr in declination for NGC 2264. The mean value of the cluster reddening is rather low and lies at $E(B-V) = 0.071 \pm 0.033$ mag (Sung et al. 1997); the differential reddening across NGC 2264 is negligible.

The age of NGC 2264 can only be determined with a relatively large error as its main sequence consists only of massive O and B stars and stars of later spectral types that are still in their PMS phase. Therefore, different values for the cluster's age are reported in the literature; they range from 3 to 10 million years (e.g., Sung et al. 2004; Sagar et al. 1986).

The V = 11.3 mag bright star HD 261711 (NGC 2264 39; GSC 00746-01783) has a spectral type of A2V (Skiff 2005) and a $(B - V)$ value of 0.13 mag (including a reddening of $E(B - V) = 0.071$ mag as given by Sung et al. 1997). According to these parameters, HD 261711 falls into the (PMS) instability strip for δ Scuti-type pulsation. The star is located in the outer part of NGC 2264 at $\alpha_{2000} = 6^{\rm h} 40^{\rm m} 16.18^{\rm s}$, $\delta_{2000} = +9° 17'$ 13.14', but with proper motion values of -3.00 ± 2.60 mas/yr in right ascension and -4.20 ± 2.40 mas/yr in declination (Høg et al. 2000) it is likely to be a cluster member.

During their evolution from the birthline to the zero-age main sequence (ZAMS), PMS stars cross different instability regions in the Hertzsprung-Russell (HR)-diagram, hence can become vibrationally unstable (e.g., Marconi & Palla 1998; Bouabid et al. 2011). Intermediate mass PMS stars with spectral types from A to early F are frequently found to show δ Scuti-like pulsation (e.g., Zwintz 2008).

In the past, extensive ground- and space-based photometric campaigns have discovered many hundreds of "classical" (post-) main sequence δ Scuti stars. δ Scuti-type pulsation frequencies are typically in the range between about 5 d^{-1} and up to 80 d^{-1}, and have p-modes driven by the κ-mechanism operating in the H, He I and He II ionization zones. Statistically, the photometrically observed modes are not distributed randomly, but cluster around the frequencies of the radial modes over many radial orders (Breger et al. 2009). Such regular frequency spacings might be explained, for example, by modes trapped in the stellar envelope (Breger et al. 2008) or by combination modes (Breger et al. 2011).

For asteroseismic modeling the identification of the modes is essential, but very often this is only possible for few of the observed frequencies. Therefore, the recognition of regularities in the observed pulsation frequency spectra is an important additional tool. Recently, several pre- and (post-) main sequence δ Scuti stars which show regular frequency patterns have been discovered, such as HD 144277 (Zwintz et al. 2011b), KIC 9700322 (Breger et al. 2011) and HD 34282 (Casey et al. 2012).

In 2006, the MOST space telescope observed NGC 2264 for the first time with the purpose to search for pulsating PMS stars. Indeed, four new PMS δ Scuti stars were revealed and the two known PMS pulsators, V 588 Mon and V 589 Mon, were confirmed (Zwintz et al. 2009). HD 261711 is among the four PMS pulsators discovered then and was denoted as "V2" in Zwintz et al. (2009). Two δ Scuti-type pulsation frequencies were revealed for HD 261711 in the 2006 MOST data (Zwintz et al. 2009).

In this study we combine the already published time series photometry of HD 261711 obtained with the MOST satellite in 2006 with recent MOST observations conducted in 2011/12 and with high-precision data from the CoRoT satellite observed in 2008 and 2011/12. We use a high-resolution spectrum to determine the atmospheric parameters and chemical abundances of HD 261711, investigate the star's location in the HR-diagram, conduct an asteroseismic investigation of the observed frequencies and discuss HD 261711's evolutionary stage.

2. MOST observations and data reduction

The MOST space telescope (Walker et al. 2003) was launched on 30 June 2003 into a polar Sun-synchronous circular orbit. At an altitude of 820 km it revolves around the Earth with a period of 101.413 min. The satellite carries a 15-cm Rumak-Maksutov telescope which feeds a CCD photometer through a single, custom broadband filter (wavelength range from 3500 to 7500 Å). MOST has successfully observed numerous objects over the past 9 years of its continuing operation.

Three types of photometric data are provided simultaneously by the MOST space telescope for different targets in its field of view. Data obtained in Fabry imaging mode are generated by a projection of the entrance pupil of the telescope – illuminated by a bright ($V < 6$ mag) target star – onto the science CCD by a Fabry microlens (see Reegen et al. 2006 for details). Direct Imaging is used for stars in the open area of the CCD which is not covered by the Fabry microlens array field stop mask. It resembles conventional CCD photometry where photometry is obtained from defocussed images of stars. Although originally not intended for scientific purposes, the MOST Guide Stars used for the attitude control system (ACS) provide highly accurate photometry which has been frequently used in the past (e.g., Zwintz et al. 2009).

MOST observed NGC 2264 including its member HD 261711 for the first time from December 7, 2006, to January 3, 2007, in a dedicated observing run on the cluster itself (Zwintz et al. 2009). The second MOST observing run on NGC 2264 lasted from December 5, 2011, to January 14, 2012, and was conducted as part of the CSI NGC 2264 (Coordinated Synoptic Investigation of NGC 2264) project together with the space telescopes CoRoT (Baglin 2006), *Spitzer* (Werner et al. 2004) and *Chandra* (Weisskopf et al. 2002). Note that HD 261711 was not observed by the *Spitzer* and *Chandra* satellites during this campaign, i.e., only measurements in the optical from MOST and CoRoT are available.

Due to the magnitude range ($7 < V < 12$ mag) and the large number of targets, in both runs NGC 2264 was observed in the open field of the MOST Science CCD in Guide Star Photometry

Table 1. Characteristics of the MOST and CoRoT observations of HD 261711.

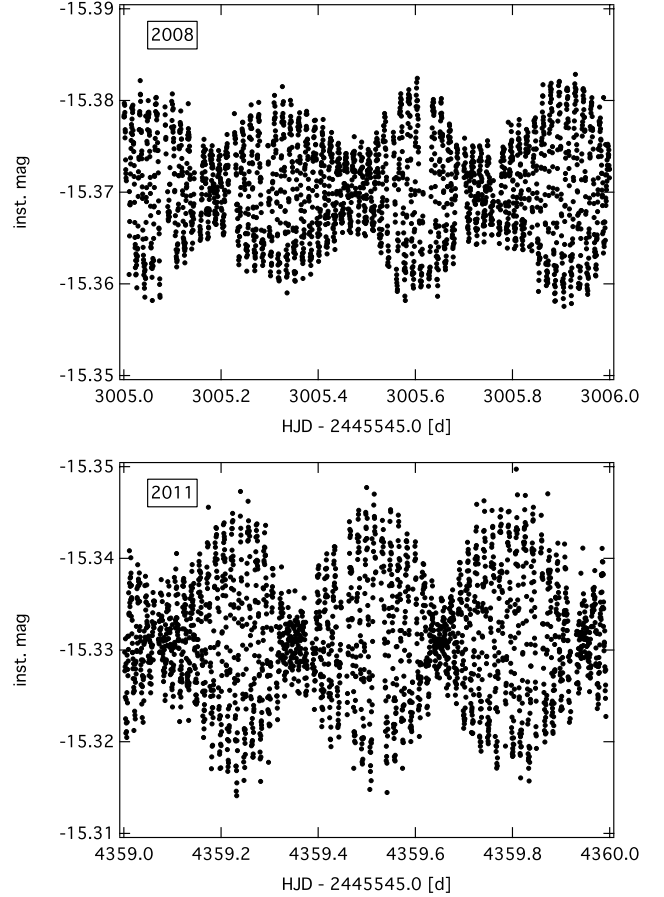| Data set	Data points #	Tbase [d]	$1/T$ [d^{-1}]	$f_{Nyquist}$ [d^{-1}]	Noise$_{res}$ [mmag]
MOST06	10 531	22.72	0.044	1362.23	0.752
MOST11/12	8391	39.98	0.025	705.40	0.757
CoRoT08	49 345	20.81	0.048	1337.21	0.014
CoRoT11/12	91 168	38.69	0.025	1221.31	0.009

Notes. Data set, number of data points used for the analysis, time base, Rayleigh frequency resolution $1/T$, Nyquist frequency and noise level of the residuals (noise$_{res}$).
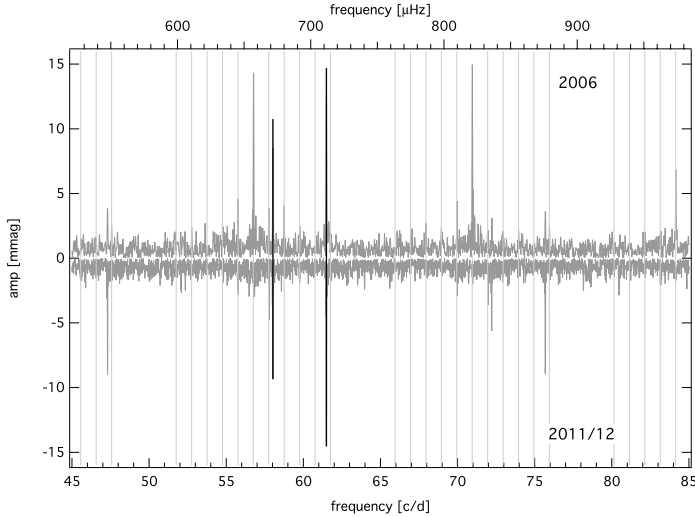
Fig. 1. MOST data for HD 261711: amplitude spectra from 45 to 85 c/d obtained in 2006 (*top panel*) and 2011/12 (*bottom panel*). The top X axes give the frequencies in μHz.

Fig. 2. One-day subsets of the CoRoT light curves obtained in 2008 (*top panel*) and 2011/12 (*bottom panel*) to the same scales.

Mode. Because not all of the candidate PMS pulsators (i.e., A and F type cluster stars) could be reached using a single pointing of the satellite, two fields of observations were chosen and observed in alternating halves of each 101-min orbit. Using this setting, MOST time series photometry was obtained for a total of 68 stars in the region of NGC 2264 in the 2006 run (Zwintz et al. 2009) and 67 in the 2011/12 run.

The corresponding MOST 2006 light curve of HD 261711 used for the analysis has a time base of ~22.7 d. The on-board exposure time was 1.5 s, 16 consecutive images were "stacked" on board resulting in an integration time of 24 s (see also Zwintz et al. 2009). The total length of the HD 261711 data set from the 2011/12 run is 39.98 d. In 2011/12 on-board exposures were 3.01 s long (to satisfy the cadence of guide star ACS operations), and the integration time was 51.17 s as 17 consecutive images were "stacked" on board.

Data reduction of the MOST Guide Star photometry was conducted using the method developed by Hareter et al. (2008) which uses a similar approach as for targets observed in Fabry imaging mode (Reegen et al. 2006), i.e., resolving linear correlations between the intensity of the target and background pixels. Since MOST Guide Star photometry does not provide information on the intensity of the background, the correlations between constant and variable stars are used instead. In a first step, the MOST Guide Stars are classified into variable and constant objects by a quick-look analysis. The data of all selected intrinsically constant objects are then combined to a comparison light curve.

Stray light effects are corrected by subtraction of linear correlations between target and comparison time-series. It is self-evident that comparison time-series are assumed and required to contain no variable stellar signal. If one of the stars used for the comparison light curve turns out to be variable (even at low amplitude levels) in a later stage of the analysis, the complete reduction has to be repeated omitting the variable star. After the Guide Star photometry reduction, the 2006 light curve of HD 261711 consists of 10531 data points, and the 2011/12 light curve has 8391 data points corresponding to Nyquist frequencies of 1362.23 d^{-1} and 705.40 d^{-1}, respectively. Note that the 2011/12 light curve has fewer data points than the 2006 light curve although the time base is significantly longer. The reason is that in 2011/12 HD 261711 was observed in the part of the orbit affected by worse stray light conditions than in 2006, hence more data points had to be discarded in the reduction.

An overview of the properties of the MOST observations is given in Table 1. The respective amplitude spectra from 2006 and 2011/12 are shown in Fig. 1. Note that the peaks between 70 and 75 d^{-1} and between 45 and 50 d^{-1} are alias frequencies to F1 and F2 with the MOST orbital frequency and disappear after prewhitening F1 and F2.

3. CoRoT observations and data reduction

The CoRoT satellite (Baglin 2006) was launched on December 27, 2006, from Baikonur aboard a Soyuz rocket into a polar, inertial circular orbit at an altitude of 896 km. CoRoT carries a 27-cm telescope and can observe stars inside

Table 2. Results from the frequency analysis of HD 261711 using MOST and CoRoT data.

Data set	F #	Frequency [d^{-1}]	[μHz]	amp$_1$ [mmag]	S/N_1	sig$_1$	amp$_2$ [mmag]	S/N_2	sig$_2$	amp$_2$ – amp$_1$ [mmag]	lin. combi.
MOST	F1	61.498(2)	711.78(2)	14.817	18.6	127.9	14.525	20.3	144.9	−0.292	
	F2	58.027(3)	671.60(4)	10.400	9.8	68.6	9.335	11.5	62.9	−1.065	
CoRoT	F1	61.4976(2)	711.778(3)	7.392	535.9	6618.6	8.103	24.0	11786.7	0.711	
	F2	58.0272(2)	671.611(3)	4.850	319.6	7391.6	5.230	63.8	12512.9	0.380	
	F3	61.4401(5)	711.112(6)	1.298	94.1	1661.9	1.435	83.0	2457.7	0.137	
	F4	58.5821(6)	678.034(7)	0.988	67.1	1311.8	1.103	19.3	1774.1	0.115	
	F5	58.0553(8)	671.937(9)	1.027	66.7	1459.3	0.966	30.8	1126.7	−0.061	
	F6	55.4566(7)	641.858(8)	0.937	56.5	1330.7	0.928	19.1	1441.3	−0.009	
	F7	55.0608(7)	637.278(9)	0.710	42.9	928.6	0.866	33.1	1191.9	0.156	
	F8	58.429(1)	676.26(1)	0.599	39.7	740.1	0.589	42.9	644.4	−0.010	
	F9	48.982(1)	566.92(1)	0.401	32.4	356.8	0.506	60.3	505.9	0.105	
	F10	55.366(2)	640.81(2)	0.348	21.1	286.2	0.334	20.8	220.6	−0.014	F3+F9-F7
	F11	51.217(4)	592.79(5)	0.135	10.2	50.8	0.134	9.7	35.8	−0.001	
	F12	54.742(4)	633.58(5)	0.164	10.3	82.3	0.130	11.1	37.9	−0.034	F11+F4-F7
	F13	53.131(5)	614.94(6)	0.100	6.7	29.1	0.119	9.1	28.5	0.019	
	F14	61.281(5)	709.27(6)	0.052	3.7	16.3	0.112	8.5	25.3	0.060	
	F15	52.057(5)	602.51(6)	0.149	10.4	65.3	0.110	8.3	24.4	−0.039	
	F16	52.374(5)	606.18(6)	0.177	12.9	83.9	0.109	10.2	25.3	−0.068	
	F17	55.891(6)	646.89(7)	0.096	5.9	24.8	0.092	8.8	16.5	−0.004	
	F18	58.231(6)	673.97(7)	0.091	5.9	29.9	0.090	7.4	16.6	−0.001	
	F19	54.808(6)	634.35(7)	0.089	5.6	19.0	0.088	8.5	15.9	−0.001	
	F20	45.739(7)	529.39(8)	0.063	4.8	10.9	0.079	8.8	13.5	0.016	
	F21	61.463(7)	711.38(9)	0.113	8.2	8.4	0.077	6.8	11.8	−0.036	F3+F5-F2
	F22	64.764(8)	749.6(1)	0.100	7.9	27.3	0.066	6.5	9.5	−0.034	
	F23	83.84(1)	970.3(1)	0.066	4.4	8.6	0.056	6.6	6.6	−0.010	
	F24	61.34(1)	709.9(1)	0.063	4.6	8.1	0.046	4.4	6.4	−0.017	F1+F14-F3
	F25	57.971(8)	670.96(9)	0.050	3.3	9.7	0.045	4.0	10.2	−0.005	

Notes. Pulsation frequencies, amplitudes, signal-to-noise values and SigSpec significances identified from the MOST data sets from 2006 (amp$_1$, S/N_1, sig$_1$) and 2011/12 (amp$_2$, S/N_2, sig$_2$) and the CoRoT data sets from 2008 (amp$_1$, S/N_1, sig$_1$) and 2011/12 (amp$_2$, S/N_2, sig$_2$) as well as the the corresponding amplitude differences (amp$_2$ – amp$_1$). The respective last-digit errors of the frequencies computed according to Kallinger et al. (2008) are given in parentheses. Possible linear combinations are given in the last column (lin. combi).

two cones of 10° radius, one at RA = 06:50 and the other at RA = 18:50. The field of view of the telescope is almost circular with a diameter of 3.8° and the filter bandwidth ranges from 3700 to 10 000 Å.

CoRoT observed NGC 2264 for the first time for 23.4 d in March 2008 during the Short Run SRa01 within the framework of the Additional Programme (Weiss 2006). A second run on the cluster NGC 2264 (SRa05) was conducted in December 2011/January 2012 with a time base of about 39 d as part of the previously mentioned CSI NGC 2264 project including also the satellites MOST, *Spitzer* and *Chandra*.

For both observing runs, the complete cluster was placed in one Exofield CCD and data were taken for all stars in the accessible magnitude range, i.e., from 10 to 16 mag in *R*. The 100 brightest stars in the field of NGC 2264 were primary targets to search for stellar pulsations among PMS cluster members.

The reduced N2 data for HD 261711 were extracted from the CoRoT data archive. The CoRoT data reduction pipeline (Auvergne et al. 2009) flags those data points that were obtained during passages of the satellite over the South Atlantic Anomaly (SAA). We did not use these "SAA-flagged" data points in our analysis. The light curve of HD 261711 obtained in 2008 consists of 49345 data points with a sampling time of 32 s. The 2011/12 data set of HD 261711 has been again observed with a sampling time of 32 s and comprises 91168 data points. One-day subsets of the CoRoT light curves from 2008 and 2011/12 are shown in Fig. 2. Table 1 summarizes the characteristics of the CoRoT light curves.

4. Frequency analysis

For the frequency analyses of all four data sets, we used the software package Period04 (Lenz & Breger 2005) that combines Fourier and least-squares algorithms. Frequencies were then prewhitened and considered to be significant if their amplitudes exceeded four times the local noise level in the amplitude spectrum (i.e., 4 S/N; Breger et al. 1993; Kuschnig et al. 1997).

We verified the analysis using the SigSpec software (Reegen 2007). SigSpec computes significance levels for amplitude spectra of time series with arbitrary time sampling. The probability density function of a given amplitude level is solved analytically and the solution includes dependences on the frequency and phase of the signal.

Each data set was analyzed independently and the results were then compared to each other.

The two MOST light curves of HD 261711 were obtained only during half-orbits and HD 261711 with a *V* magnitude of 11.3 is a rather faint target for the MOST space telescope. In the frequency analysis of the MOST light curve from 2006, only two frequencies were attributed to pulsation; the other peaks are connected to the orbital frequency of the satellite, its harmonics and 1 d^{-1} sidelobes (Zwintz et al. 2009). These two pulsation frequencies, i.e., F1 at 61.498 ± 0.002 d^{-1} (711.78 ± 0.02 μHz) and F2 at 58.027 ± 0.003 d^{-1} (671.60 ± 0.04 μHz) are confirmed in the 2011/12 data set (see Fig. 1 and Table 2) and no additional peaks originating from pulsation could be found. The residual noise levels for the two MOST light curves from 2006
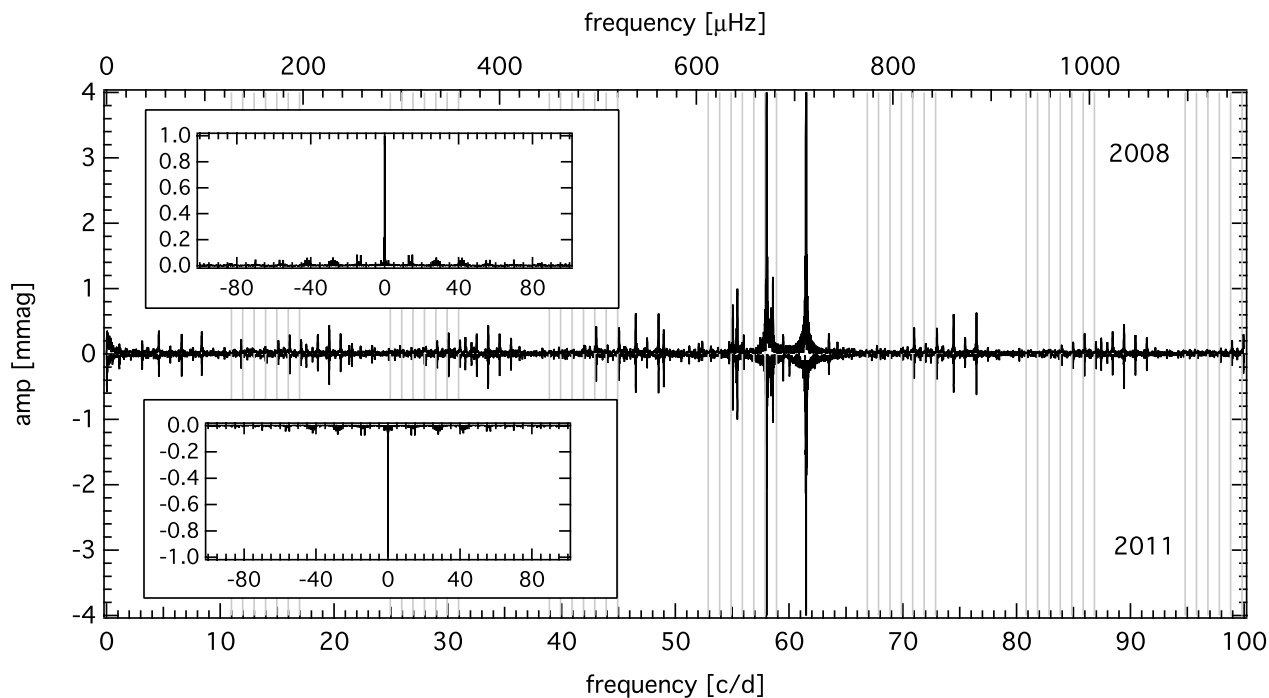
Fig. 3. Original amplitude spectra of the CoRoT data obtained in 2008 (pointing upwards) and 2011/12 (pointing downwards) from 0 to 100 d^{-1} (i.e., from 0 to 1157.4 μHz) and zoomed in amplitude to 4 mmag. The corresponding spectral window functions are given as inserts, respectively.

and 2011/12 after prewhitening all significant frequencies are 0.752 and 0.757 mmag, respectively.

In the CoRoT photometry, the influence of the satellite's orbital and related frequencies has to be taken into account as well, but the effects are less than for the MOST time series. The complete amplitude spectra for both years from 0 to 100 d^{-1} with a zoom in amplitude up to 4 millimag are given in Fig. 3 with the corresponding spectral window functions given as insets. The frequency analyses of the CoRoT light curves from 2008 and 2011/12 yielded 25 common frequencies which were attributed to pulsation. The two frequencies found in the MOST data sets, F1 and F2, were confirmed using the CoRoT data. Table 2 lists all frequencies together with the amplitudes derived from the different years and including the last digit errors given in parentheses computed according to Kallinger et al. (2008). Figure 4 shows zooms into the two amplitude spectra of the original data sets (top panels), residuals after prewhitening with the two highest amplitude frequencies, F1 and F2 (middle panels) and residuals after prewhitening the first ten frequencies. The corresponding 25 pulsation frequencies are identified as solid black lines. After prewhitening all significant frequencies the residual noise levels of the 2008 and 2011/12 data sets are 13.7 ppm and 9.15 ppm, respectively. The residuals are shown in Fig. 5.

Figure 4 illustrates the presence of regular patterns of groups of frequencies with nearly equidistant spacing. Similar effects have been observed in other δ Scuti-type stars, such as in HD 144277 (Zwintz et al. 2011b) and HD 34282 (Casey et al. 2012). The pulsation frequencies of all three objects are rather high and with similar separations of the groups of observed frequencies lying between 3 and 4 d^{-1}. All three stars are also hot objects close to the blue border of the instability region for (PMS) δ Scuti-type stars.

5. Spectroscopic analysis

To model the frequencies detected in the light curves of HD 261711, we analysed a high resolution spectrum

($R \sim 52\,000$) obtained with the Robert G. Tull Coudé Spectrograph (TS), mounted on the 2.7-m telescope of Mc Donald Observatory. The spectrum was obtained on 2010, December 2nd, and covers the 3633–10 849 Å wavelength range with gaps between the échelle orders at wavelengths longer than 5880 Å. Adopting an exposure time of 90 min we obtained a signal-to-noise ratio (S/N) per pixel, calculated over 1 Å at ~5000 Å, of about 100.

Bias and flat field frames were obtained at the beginning of each night, while several Th-Ar comparison lamp spectra were obtained each night for wavelength calibration purposes. The reduction was performed using the Image Reduction and Analysis Facility (IRAF)[1]. The spectra were normalised by fitting a low order polynomial to carefully selected continuum points.

We simultaneously used hydrogen lines and metallic lines to estimate the star's effective temperature ($T_{\rm eff}$) and surface gravity ($\log g$). The TS spectrum, in the adopted configuration, covers fully the Hγ and Hβ lines, but the latter cannot be used because it is affected by a defect of the spectrograph's imaging system. Because of gaps in the spectral orders in the red, the Hα line is not fully covered. We normalised the Hγ line using the artificial flat-fielding technique described in Barklem et al. (2002), which has already proven to be successful with TS data (Fossati et al. 2011b). To supplement the Hγ observation acquired at Mc Donald Observatory, we obtained a low resolution ($R \sim 15\,000$) spectrum, covering Hα (6470–6710 Å), with the 1.8-m telescope of the Dominion Astrophysical Observatory (Canada). Low resolution spectra allow a better control of the normalisation, decreasing therefore the systematics which might be introduced by considering the Hγ line, only. We reduced the DAO spectrum with IRAF in a similar way as the TS spectrum.

---

[1] IRAF (http://iraf.noao.edu) is distributed by the National Optical Astronomy Observatory, which is operated by the Association of Universities for Research in Astronomy (AURA) under cooperative agreement with the National Science Foundation.
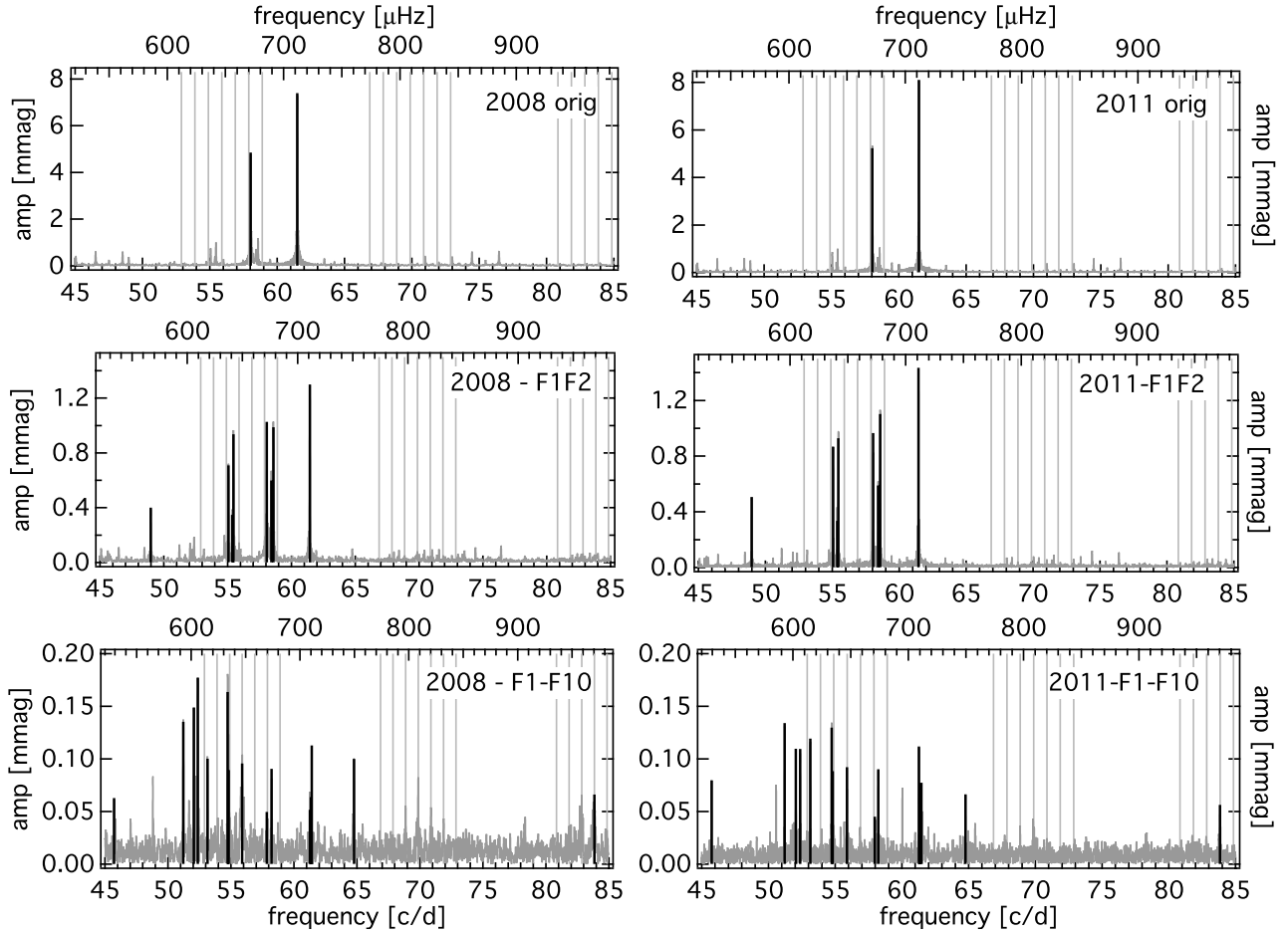
Fig. 4. CoRoT data for HD 261711: original amplitude spectra from 45 to 85 c/d obtained in 2008 (*left*) and 2011/12 (*right*) with F1 and F2 marked, residual amplitude spectra after prewhitening F1 and F2 where F3 to F10 are marked (*middle panels*) and residual amplitude spectra after prewhitening F1 to F10 showing F11 to F25. The top *X* axes give the frequencies in μHz.

To compute model atmospheres of HD 261711 we employed the LLMODELS stellar model atmosphere code (Shulyak et al. 2004). We analysed the hydrogen lines fitting synthetic spectra, calculated with SYNTH3 (Kochukhov 2007), to the observed line profiles. The hydrogen lines did not allow a very precise T_{eff} determination, leading to a best fitting temperature of 8600 ± 400 K; in this temperature regime hydrogen lines have little reaction to T_{eff} variations. On the other hand, we were able to better determine $\log g$ to a value of 4.1 ± 0.2.

We further constrained T_{eff} and $\log g$ making use of the Fe excitation and ionisation equilibria. This allowed us to improve the T_{eff} determination, obtaining finally 8600 ± 200 K, and to confirm the $\log g$ value of 4.1 ± 0.2, previously obtained with the analysis of the hydrogen lines. Figures 6 and 7 show a comparison between observed and synthetic profiles, calculated with the final adopted parameters, for the Hγ and Hα lines, respectively. We also show here synthetic profiles calculated by increasing/decreasing $\log g$ by 0.2 dex (Fig. 6), and T_{eff} by 200 K (Fig. 7). Our fundamental parameters provide the best overall description of the available observables: hydrogen and metallic line profiles. As Table 3 shows, within the uncertainties we obtained the ionisation equilibrium also for elements other than Fe, such as Mg and Si.

By fitting synthetic spectra to several weakly blended lines, we measured a $\upsilon \sin i$ of 53 ± 1 km s^{-1}. The local thermodynamic equilibrium (LTE) abundance analysis was based on equivalent widths, analysed with a modified version (Tsymbal 1996) of the
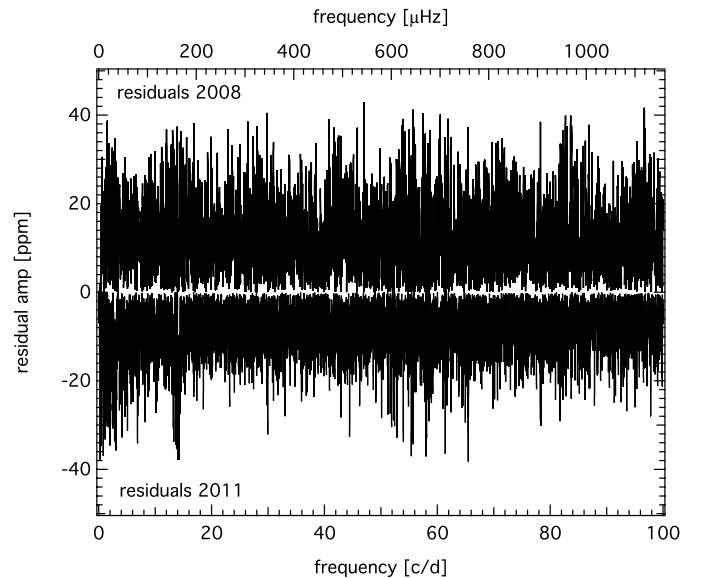

Fig. 5. Residuals of the CoRoT data from 2008 (pointing upwards) and 2011/12 (pointing downwards) after prewhitening all significant frequencies. Note that the *Y* axis is given in ppm.

WIDTH9 code (Kurucz 1993). The relatively large $\upsilon \sin i$ value did not allow us to measure, with classical methods (e.g., direct integration and line profile fitting; Fossati et al. 2009), the
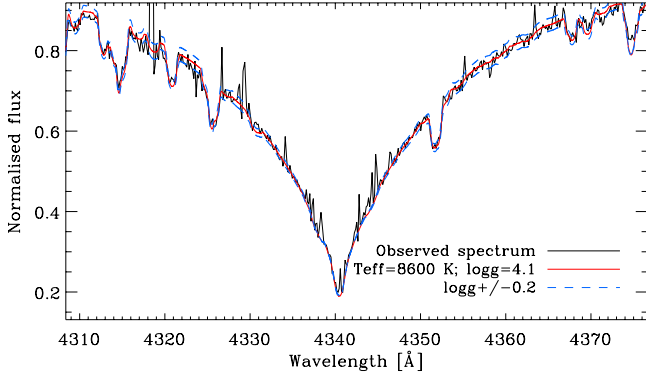
Fig. 6. The region of the Hγ line for HD 261711: observed spectrum (black solid line), synthetic spectrum with the final adopted stellar parameters (T_{eff} = 8600 K, $\log g$ = 4.1 – red thick solid line) and synthetic spectra calculated by increasing/decreasing $\log g$ by 0.2 dex (blue dashed lines).
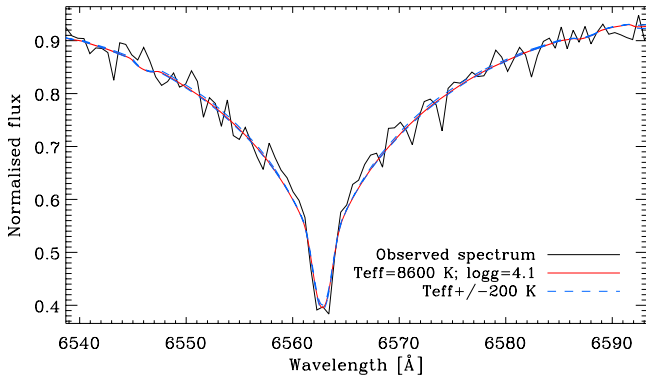
Fig. 7. The region of the Hα line for HD 261711: observed spectrum (black solid line), synthetic spectrum with the final adopted stellar parameters (T_{eff} = 8600 K, $\log g$ = 4.1 – red thick solid line) and synthetic spectra calculated by increasing/decreasing T_{eff} by 200 K (blue dashed lines). Note that the three synthetic spectra overlap because of the little reaction of the Hα line to T_{eff} variations in this temperature regime.

equivalent width of a statistically large enough number of lines. For this reason, we derived the equivalent widths of the unblended and several weakly blended lines making use of an average line profile, calculated with the least-squares deconvolution (LSD) technique (Donati et al. 1997, Kochukhov et al. 2010). We iteratively fitted the observed spectrum by placing the LSD profile at the wavelength position of the various spectral lines, using as free parameter only the depth of the LSD profile. The equivalent width of the LSD profile, scaled with the fitted line depth, gives the line equivalent width. The method we adopted here to measure the equivalent widths of weakly blended lines will be described in detail in a separate work (Fossati et al., in prep.).

We determined the microturbulent velocity (v_{mic}) applying the equilibrium between abundance and equivalent widths for all measured Fe I lines, obtaining v_{mic} = 3.0 ± 0.5 km s^{-1}. We determined the abundances of 15 elements, listed in Table 3, obtaining values comparable to solar and in agreement within the errors with the overall cluster metallicity of −0.15 dex (Lynga 1987). In Table 3 we also listed for comparison the abundances we derived for NGC 2264 VAS 20 and NGC 2264 VAS 87 (Zwintz et al. 2013), two other members of the NGC 2264 open cluster. The abundance pattern of the three stars is comparable within the

Table 3. LTE atmospheric abundances of HD 216711 with the error estimates based on the internal scatter from the number of measured lines, n.

Ion	HD 216711		VAS 20	VAS 87	Sun
	$\log(N/N_{tot})$	n	$\log(N/N_{tot})$		
C I	−3.43 ± 0.04	5			−3.61
Na I	−5.53 ± 0.13	2	−5.83	−5.68	−5.87
Mg I	−4.46 ± 0.13	4	−4.63	−4.55	−4.44
Mg II	−4.42 ± 0.10	2			−4.44
Si I	−4.59:	1	−4.58	−4.87	−4.53
Si II	−4.47 ± 0.10	5	−4.49		−4.53
Ca I	−5.65 ± 0.12	11	−5.64	−5.71	−5.70
Ca II	−5.85 ± 0.13	2			−5.70
Sc II	−9.12 ± 0.08	4	−8.97	−9.16	−8.89
Ti II	−7.20 ± 0.10	6	−7.03	−7.14	−7.09
Cr I	−6.86 ± 0.05	3	−6.37	−6.39	−6.40
Cr II	−6.38 ± 0.11	7	−6.44	−6.06	−6.40
Mn I	−6.36 ± 0.23	3	−6.36	−6.44	−6.61
Fe I	−4.62 ± 0.20	45	−4.55	−4.63	−4.54
Fe II	−4.61 ± 0.14	27	−4.52	−4.58	−4.54
Ni I	−5.88 ± 0.11	3	−5.77	−5.83	−5.82
Sr II	−9.56:	1			−9.17
Y II	−9.60:	1	−9.94	−9.66	−9.83
Zr II	−9.10:	1			−9.46
Ba II	−9.52 ± 0.32	3	−9.29	−9.51	−9.86
T_{eff}	8600 K		6380 K	6220 K	5777 K
$\log g$	4.1		4.0	3.8	4.44

Notes. For comparison purpose, columns 4,5 and 6 list respectively the abundances obtained by Zwintz et al. (2013) for NGC 2264 VAS 20 and NGC 2264 VAS 87 and for the Sun (Asplund et al. 2009).

uncertainties, as expected for members of the same open cluster, though with rather different temperatures (Fossati et al. 2011a).
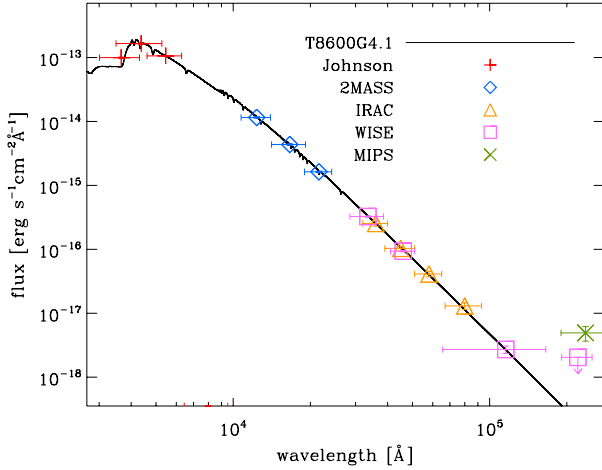
5.1. Spectral energy distribution

Figure 8 shows the fit of the synthetic fluxes, calculated with the fundamental parameters given before, to the observed Johnson (Mermilliod et al. 1994), 2MASS (Zacharias et al. 2005), *Spitzer* (IRAC – Sung et al. 2009), WISE (Cutri et al. 2012) and MIPS (Sung et al. 2009) photometry, converted to physical units. We converted the photometry adopting the calibrations provided, respectively, by Bessel et al. (1998), van der Bliek et al. (1996), the *Spitzer* IRAC instrument handbook[2], Wright et al. (2010) and the *Spitzer* MIPS instrument handbook[3]. Adopting the cluster distance and reddening given by Sung et al. (1997), we estimated a stellar radius of 1.8 ± 0.5 $R_{\odot}$. This comparison also confirms the temperature we obtained for HD 261711. Using the T_{eff} value of 8600 K derived from the spectrum analysis and the radius of 1.8 $R_{\odot}$, the luminosity $\log L/L_{\odot}$ for HD 261711 evaluates to 1.20 ± 0.14.

Note that for the reddest WISE photometric point only an upper limit is available in the literature which is illustrated with small arrows in Fig. 8. But an increased flux is also detected in the MIPS measurement which agrees to the higher flux seen in the reddest WISE photometric point. The excess in the infrared indicates that HD 261711 might still be surrounded by remnants

---

[2] http://irsa.ipac.caltech.edu/data/SPITZER/docs/irac/iracinstrumenthandbook/

[3] http://irsa.ipac.caltech.edu/data/SPITZER/docs/mips/mipsinstrumenthandbook/

Fig. 8. Comparison between LLMODELS theoretical fluxes (full line), calculated with the fundamental parameters derived for HD 261711, with Johnson (crosses), 2MASS (diamonds), *Spitzer* IRAC (triangles), WISE (squares), and MIPS (cross) photometry converted to physical units. The horizontal lines indicate the wavelength range covered by each photometric point.

of its birth cloud. This illustrates the relative youth of the star and, thus, supports its membership to NGC 2264.

Using the radius of $1.8 R_\odot$ and the $\upsilon \sin i$ of 53 km s^{-1}, the longest possible rotation period is 1.72 d, i.e., 0.56 d^{-1} (6.5 μHz). Hence, it is unlikely that the observed spacing between groups of frequencies corresponds to rotational splitting. We will discuss possible explanations of the observed spacings in the following section.

6. Asteroseismic modeling

HD 261711 presents an interesting pulsation spectrum in which the frequencies appear in groups. The separation in frequency between each group is equal to the large frequency spacing for a star occupying HD 261711's location in the HR diagram. This pattern is similar to that found in PMS stars HD 34282, analyzed by Casey et al. (2012, hereafter, CZG), and HD 144277 (Zwintz et al. 2011b). CZG found that the frequency separation between the weighted group-averaged frequencies corresponds to the large spacing predicted by the stellar models. CZG were unable to explain why the radial modes (apparently) split into groups of multiple frequencies. They considered rotational splittings, higher order l-values, and amplitude modulations of short-lived modes as the cause. They were able to rule out rotational splittings and higher order l-values but were unable to resolve the spectrum as a function of time well enough to see if any evidence for varying amplitudes existed.

Our analysis of HD 261711's oscillation spectrum follows the approach taken by CZG. We first identify the principle groups and then compute the weighted averaged frequency for each group G_j according to:

$$G_j = \frac{\sum_{i=1}^{N_j} f_{ji} a_{ji}}{\sum_{i=1}^{N_j} a_{ji}}, \tag{1}$$

where a_{ji} and f_{ji} are the ith amplitude and frequency of the frequencies in the jth group and N_j is the number of frequencies in the jth group. Values were taken from the CoRoT 2011/12 observations due to the highest accuracies in frequencies and

Table 4. Frequency group label, weighted average frequency, the CoRoT observed pulsation label and frequency (from Table 2) sorted by increasing frequency.

| Group	Weighted frequency [μHz]	Frequency label	Frequency [μHz]
G01	529.39	F20	529.39
G02	566.92	F09	566.92
G03	603.33	F11	592.79
		F15	602.51
		F16	606.18
		F13	614.94
G04	639.75	F12	633.58
		F19	634.35
		F07	637.28
		F10	640.81
		F06	641.86
		F17	646.89
G05	671.94	F25	670.96
		F02	671.61
		F05	671.94
		F18	673.97
		F08	676.26
		F04	678.03
G06	711.76	F14	709.27
		F24	709.91
		F03	711.11
		F21	711.38
		F01	711.78
G07	749.59	F22	749.59
G08	970.34	F23	970.34
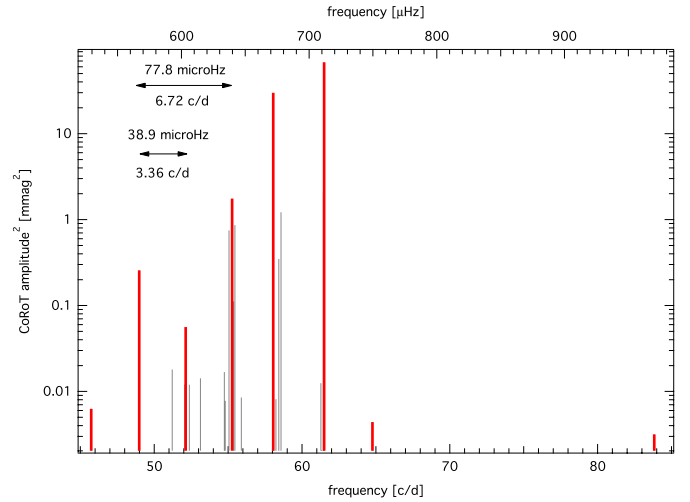
Fig. 9. Weighted (red thick lines) and observed (grey thin lines) pulsation frequencies with squared amplitudes of HD 261711 where the characteristic mean observed spacing of about 3.36 d^{-1} (38.9 μHz) and twice its value, i.e., 6.72 d^{-1} (77.8 μHz), are indicated.

amplitudes. Table 4 lists the group label, the weighted average frequency, and the included frequencies (from Table 2).

Figure 9 shows the observed 25 pulsation frequencies as thin grey lines and the weighted average frequencies as thick red lines with squared amplitudes. The observed average characteristic spacing is around 3.36 d^{-1} (38.9 μHz) which is indicated by arrows together with twice the observed spacing of about 6.72 d^{-1} (77.8 μHz).

In Fig. 10 we plot the observed frequencies and the weighted-averaged frequencies in an echelle diagram (frequency versus frequency modulo a folding frequency). The folding
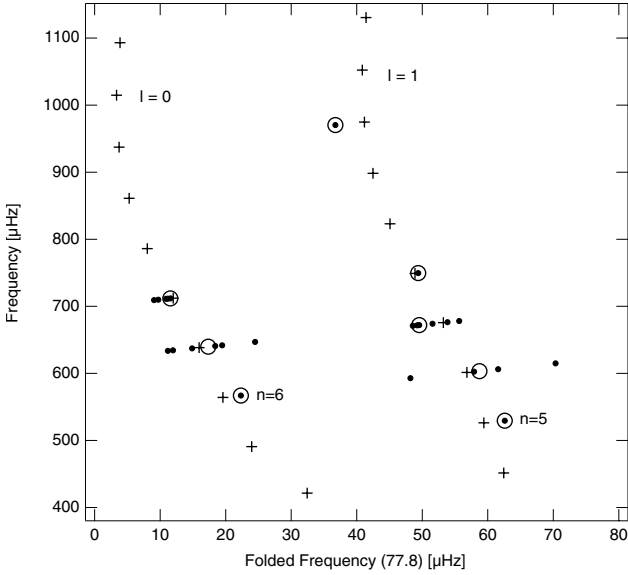
Fig. 10. Echelle diagram showing the CoRoT 2011/12 observations (small filled circles), the weighted average frequencies (large open circles), and the selected best model fit (plus symbols) with an identification of the n values from the models.

Fig. 11. HR-diagram showing the lowest χ^2 models (crosses). The models with low χ^2 and lying near the star's location in the HR-diagram are shown with filled circles whose radii are inversely proportional to χ^2. Also shown are PMS evolutionary tracks with the indicated masses ($M_\odot$) and the birthline. HD 261711's observational HR-diagram position including uncertainties was derived using the spectroscopically determined value of $\log T_{\rm eff}$ and the asteroseismic radius of 1.65 $R_\odot$.

frequency is 77.8 μHz and was chosen to produce vertically aligned ridges of modes, a signature of p-modes. The $l = 0$ and 1 p-mode frequencies of our best model fit to the weighted averaged frequencies, to be discussed below, are also shown in Fig. 10.
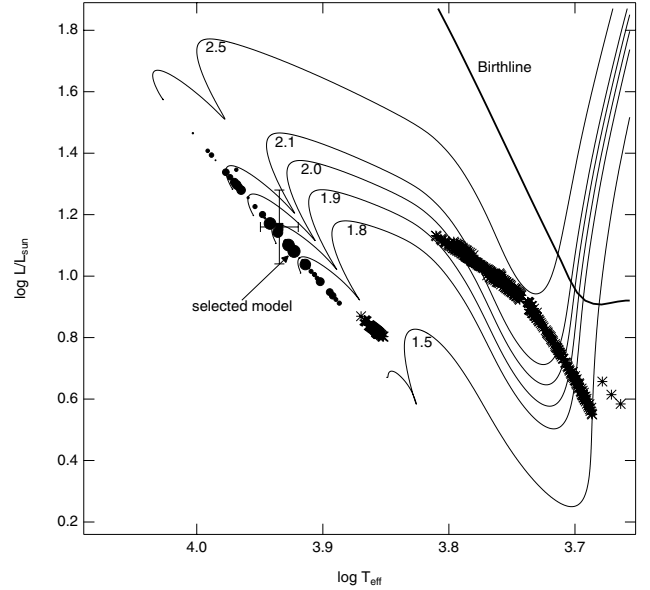
After failing to find a model whose frequencies fit all the observed frequencies, we attempted to fit a model to just the eight weighted averaged frequencies. We used the usual χ^2 fitting procedure, first described in Guenther and Brown (2004). The match between the observed and model spectra is quantified by the following χ^2 equation:

$$\chi^2 = \frac{1}{N} \sum_{i=1}^{N} \frac{(f_{\rm obs,i} - f_{\rm mod,i})^2}{\sigma^2_{\rm obs,i} + \sigma^2_{\rm mod,i}} \qquad (2)$$

where N is the number of weighted averaged frequencies, $f_{\rm obs,i}$ and $f_{\rm mod,i}$ are the ith weighted averaged and model frequencies, respectively, and $\sigma^2_{\rm obs,i}$ and $\sigma^2_{\rm mod,i}$ are the ith weighted average and model frequency uncertainties. Here we assume the model frequency uncertainties are small compared to the weighted averaged frequency uncertainties. For simplicity of modeling and because we do not have a formal explanation for the cause of the splittings within each group, we set the uncertainty of all the weighted averaged frequencies to ±1 μHz.

The model frequencies were taken from the same PMS model grid as used in Guenther et al. (2009). The model grid was constructed using the YREC stellar evolution code (Demarque et al. 2008). Solar metallicity ($Z = 0.02$) models between 1.00 and 5.00 $M_\odot$, in increments of 0.01 $M_\odot$, were used. The PMS models, themselves, lie along evolutionary tracks that start on the Hayashi track and end on the ZAMS where nuclear burning begins. The non-adiabatic stellar pulsation program by Guenther (1994) was used to calculate the adiabatic p-mode frequency spectrum of each model. Radial orders $n = 0$ to 30 and azimuthal orders $l = 0$ to 3 were compared to the weighted averaged frequencies and the models with the lowest χ^2 were identified.

Figure 11 shows the regions in the HR-diagram where the models have the lowest χ^2 (<10). The models that lie close to

HD 261711's position in the HR-diagram derived from our observations are represented by circle sizes that are inversely proportional to χ^2 with the largest circles corresponding to models whose oscillation spectra best match the weighted averaged frequencies. Two regions of models were found to fit the weighted averaged frequencies of the observed oscillation spectrum, one near the ZAMS and the other in a region below the birthline. The models near the birthline correspond to fits in which the weighted averaged frequencies correspond to purely radial or purely $l = 1$ p-modes. The best fitting models near the ZAMS correspond to fits in which the weighted averaged frequencies correspond to both $l = 0$ and 1 p-modes. At this time we do not consider further the low χ^2 models near the birthline because they do not match the stars location in the HR-diagram derived from observations.

The models that do match the weighted averaged frequencies and lie within the observed HR-diagram position of HD 261711 have masses from 1.8 $M_\odot$ to 1.9 $M_\odot$ and ages from 10 to 11 Myr (from birthline).

The asteroseismic observations and the spectroscopic observations are consistent; hence, it appears that the weighted averaged frequencies are related to the $l = 0$ and 1 p-modes. If our l-value identifications are correct then, it is not possible for the radial modes to be split by rotation; hence, rotation as a cause of the splitting is ruled out. Although we cannot completely rule out the possibility that the modes are $l = 1$ and 2, or 2 and 3 but we note that these fits have higher χ^2 than those shown here.

To see if the mode amplitudes varied during the period of observation, which could introduce spurious peaks about the parent frequency during the Fourier extraction of the star's oscillation spectrum, we split the data up into smaller subsets. Using the longest data set, i.e. the CoRoT 2011/12 observations, and splitting them in half, i.e., first ~20 d and second ~20 d with one day overlap, showed no significant amplitude changes in the modes. But when we split the same data set into nine
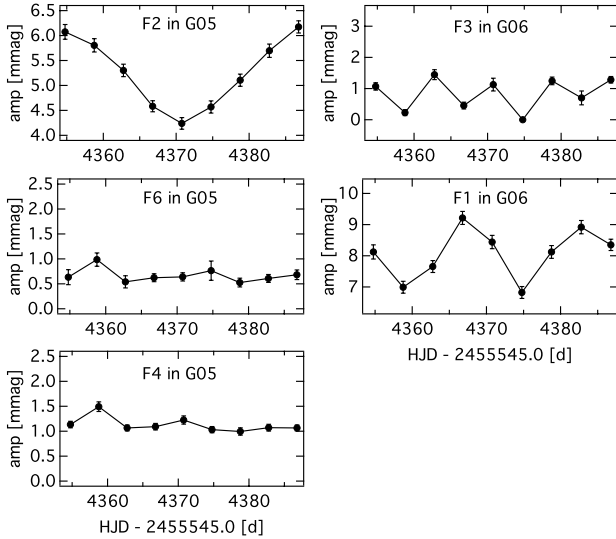
Fig. 12. Modulation of the amplitudes of frequencies F2 (*top left*), F6 (*middle left*) and F4 (*bottom left*) of group G05 and F3 (*top right*) and F1 (*middle right*) of group G06 when splitting the CoRoT 2011/12 data sets in nine subsets of ~5 d length. Amplitude errors are computed according to Kallinger et al. (2008).

subsets of five days each (to maintain some frequency resolution) with one day overlaps, we were able to resolve amplitude variations among some of the modes in G05 (three modes) and G06 (two modes), see Fig. 12. The amplitude modulations could be caused by nonlinear coupling of the modes to each other or some other periodic effect within the star or they could simply be an instrumental effect. Regardless, the observed amplitude modulation does offer a simple explanation for the apparent multiple peaks in the Fourier spectrum. The simplest interpretation of the oscillation spectrum remains, i.e., that they are radial and first order *p*-modes.

The oscillation spectrum of one of the best fitting models (shown in Fig. 11) is plotted in Fig. 10 along with the observations. The selected best fitting model has an age of 11 Myr and a radius of $1.65 R_\odot$ in agreement with the radius derived from spectral energy distribution (SED) fitting. The echelle diagrams of other best fitting models are similar at the level of our assumed uncertainties. The model fit shows that the weighted averaged frequencies for HD 261711 align along two vertical ridges in the echelle diagram corresponding to $l = 0$ and 1 *p*-modes of $n = 6$ and 5, respectively. The folding frequency of the echelle diagram is approximately equal to the large frequency spacing. Our result is consistent with Guenther et al. (2009) who first studied this star using just the two frequencies observed by MOST (see Table 2).

Comparing the best model fit to the observed frequencies and to the weighted averaged frequencies, it appears that the model fit frequencies are better aligned to the center of the groups of frequencies than the weighted averaged frequencies. Unlike the previously studied HD 34282 (CZG), HD 261711 shows both radial and nonradial *p*-modes. Also, unlike HD 34282, all the observed frequencies for HD 261711 fall well below the acoustic cutoff frequency. The observed frequencies for HD 34282 appear to extend right up to the acoustic cutoff frequency (CZG).

7. Evolutionary stage of HD 261711

Close to the ZAMS, the atmospheric properties (T_{eff}, $\log g$, luminosity and mass) of pre- and (post-) main sequence stars are
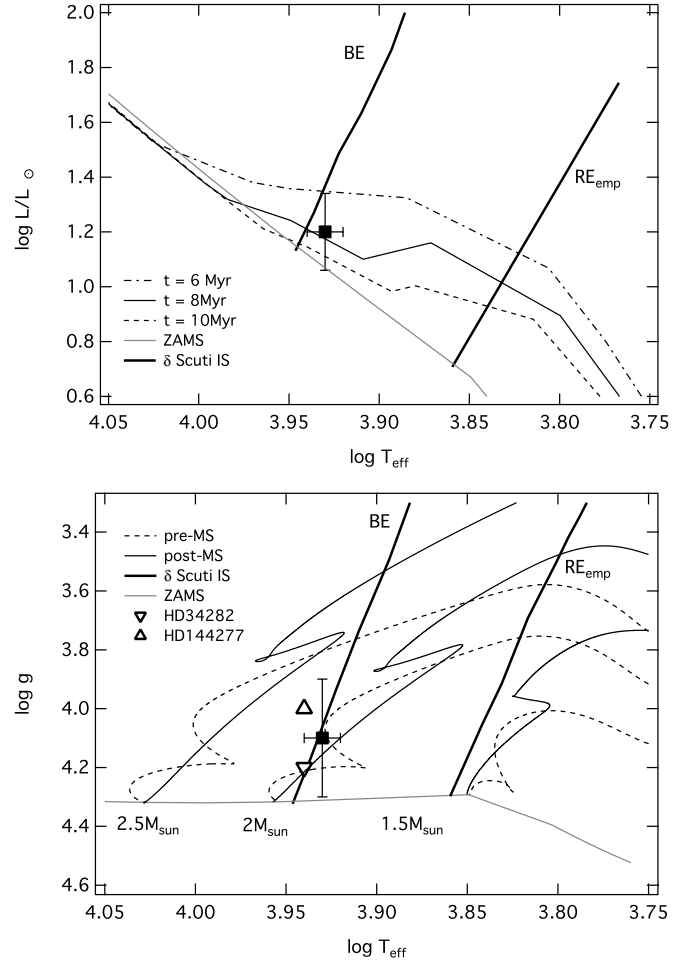
Fig. 13. Position of HD 261711 in the HR-diagram in comparison with isochrones (*top panel*) and evolutionary tracks (*bottom panel*). In both panels the ZAMS is indicated by a grey, solid line and the borders of the δ Scuti instability strip are marked with thick solid lines. The position of HD 261711 is given with a filled square. *Top panel*: isochrones with ages of 6, 8 and 10 Myr are indicated with a dash-dotted, solid and dashed line. *Bottom panel*: PMS evolutionary tracks for 1.5, 2.0 and 2.5 $M_\odot$ are shown with dashed lines, (post-)main sequence evolutionary tracks for the same masses with solid lines. The open symbols mark the positions of HD 34282 (down triangle) and HD 144277 (up triangle).

quite similar (Marconi & Palla 1998). A distinction between evolutionary stages just from the stars' positions in the HR-diagram is not possible because pre- and post-main sequence evolutionary tracks intersect close to the ZAMS (Breger & Pamyatnykh 1998). The main difference between PMS stars and their more evolved counterparts lies in their interior structures which can be investigated using asteroseismology.

The bottom panel of Fig. 13 shows the HR-diagram position of HD 261711 together with the pre- and post-main sequence evolutionary tracks for 1.5, 2.0 and 2.5 $M_\odot$, and the borders of the δ Scuti instability strip. Pre- and post-main sequence evolutionary tracks (dashed and solid lines) were taken from D. Guenther (private comm.) using the YREC evolution code (Demarque et al. 2008) with physics described in Guenther et al. (2009). The borders of the classical δ Scuti instability strip (i.e., the general blue edge, BE, and the empirical red edge, RE$_{emp}$, thick solid lines) are from Breger & Pamyatnykh (1998). The ZAMS is indicated by a grey line. The PMS δ Scuti instability strip coincides well with the classical δ Scuti instability

strip (Zwintz 2008), hence it is sufficient to plot one of the two. HD 261711 is located at the hot border of the instability region and close to the intersecting evolutionary tracks of 2.0 $M_\odot$. For comparison the positions of the two similar objects, HD 34282 (Casey et al. 2012) and HD 144277 (Zwintz et al. 2011b) are given. From this plot alone, no clear distinction of the evolutionary stage for HD 261711 (and also for HD 34282 and HD 144277) can be drawn.

Independent information about the age of the star can resolve the evolutionary state. In the case of HD 261711, we can make use of two additional pieces of information, the cluster membership and the age derived from asteroseismology.

HD 261711 is a very likely member of the young open cluster NGC 2264 according to its proper motion values of -3.00 ± 2.60 mas/yr in right ascension and -4.20 ± 2.40 mas/yr in declination (Hog et al. 2000). The corresponding values for NGC 2264 are -2.70 ± 0.25 mas/yr and -3.50 ± 0.26 mas/yr (Kharchenko et al. 2001). We determined a radial velocity of 14 ± 2 km s^{-1} for HD 261711 from our spectrum which agrees also well to the cluster radial velocity of 17.68 ± 2.2 km s^{-1} (Kharchenko et al. 2005). NGC 2264 has a maximum age of 10 million years (e.g., Sung et al. 2004; Sagar et al. 1986). Hence, all stars of spectral types later than A0 that lie above the ZAMS must be in the PMS evolutionary phase. Therefore, HD 261711 being a cluster member cannot be an evolved δ Scuti star.

The upper panel of Fig. 13 shows the HR-diagram position of HD 261711 together with isochrones of 6 (dash-dotted line), 8 (solid line) and 10 (dashed line) million years (Demarque et al. 2008). For the isochrones, we adopted the slightly less than solar metallicity reported for NGC 2264, i.e., [Fe/H] = -0.15. Under the assumption that HD 261711 is a member of NGC 2264, it can be derived from Fig. 13 that its age is about 8 ± 2 million years.

From our asteroseismic analysis, we also find that the best fitting models put the star relatively close to the ZAMS (see Sect. 6 and Fig. 11) and yield an age of 10 million years. This again is an argument that HD 261711 cannot be an evolved δ Scuti star, and the asteroseismic age fits well to the age derived from the isochrones using the star's membership in NGC 2264.

Many PMS stars show emission lines in their spectra or an increased flux in the infrared originating from the remnants of their birth clouds. In the case of NGC 2264, the dense cloud of material apparently lies behind the stars. This is supported by the presence of only small amounts of reddening across the cluster reported in the literature (e.g., Sung et al. 1997). The SED of HD 2617211 (Fig. 8) shows a slightly increased flux in the infrared that might be attributed to the presence of circumstellar material along the line of sight. We did not detect emission lines in our spectrum. This is not too surprising because several other members of NGC 2264 with properties similar to HD 261711 have been reported not to show emission in their spectra, e.g., NGC 2264 VAS 20 and NGC 2264 VAS 87 (Zwintz et al. 2013) or HD 261230 and HD 261387 (Zwintz et al. 2009).

Putting all this information together we conclude that HD 261711 is either still in its PMS phase just before arrival on the ZAMS or it is already a young main sequence star which has just started to burn hydrogen in its core.

8. Summary

High-precision time series photometry from the MOST and CoRoT satellites was obtained for HD 261711 in 2006, 2008 and 2011/12. Using these four data sets, 25 δ Scuti-type pulsation

frequencies have been discovered that lie between 45 and 84 d^{-1}, i.e., between about 520 and 972 μHz.

The observed frequencies are found in groups with a characteristic spacing of about 3.36 d^{-1} (38.9 μHz). This pattern resembles two other cases reported earlier, i.e., HD 34282 (CZG 2012) and HD 144277 (Zwintz et al. 2011b).

Using dedicated high-resolution spectroscopy we derived the atmospheric parameters and chemical abundances for HD 261711. The star has an effective temperature of 8600 $\pm$ 200 K which corresponds well to the reported spectral type of A2 found in the literature and to one of the best asteroseismic model fitting regions presented here. log g is 4.1 ± 0.2 and $v \sin i$ was found to be 53 ± 1 km s^{-1}. Chemical abundances were derived for 15 elements, are comparable to the solar values and agree within the errors to the overall cluster metallicity.

As it was not possible to fit asteroseismic models to all observed frequencies, we fitted models to the weighted averaged frequencies of the eight observed groups. Two regions of models in the HR-diagram were found to fit these eight frequencies best: one is near the birthline and includes either purely radial or purely $l = 1$ p-modes; the other is close to the ZAMS and the frequencies correspond to $l = 0$ and $l = 1$ p-modes with n values of 6 and 5, respectively. The latter model also matches the location of HD 261711 in the HR-diagram obtained from spectroscopy. Therefore, we interpret HD 261711 to show $l = 0$ and $l = 1$ p-modes, to have a mass between 1.8 and 1.9 $M_\odot$ and an age between 10 and 11 million years.

We can confirm the membership of HD 261711 to the young cluster NGC 2264 as (i) its chemical abundances agree with the overall cluster metallicity; (ii) the T_{eff} and log g values derived from spectroscopy yield HD 261711 to be a hot A star close to the ZAMS; (iii) its radial velocity agrees to the cluster values; (iv) there is an indication for an infrared excess in the SED; and (v) the age determined from asteroseismology coincides well within the uncertainties to the overall cluster age.

We now have three stars HD 34282 (CZG 2012), HD 144277 (Zwintz et al. 2011b) and HD 261711 that show a similar p-mode spectra pattern and fit our models. The appearance of multiple frequencies in groups could be a consequence of the frequency extraction process which does not allow for varying amplitude modes. We do observe amplitude modulation in some of the modes. At this time, though, we cannot say whether the amplitude modulation is intrinsic, presumably caused by some nonlinear coupling, or an instrumental effect.

References

Asplund, M., Grevesse, N., Sauval, A. J., & Scott, P. 2009, ARA&A, 47, 481
Auvergne, M., Baudin, P., Boisnard, L., et al. 2009, A&A, 506, 411
Baglin, A. 2006, The CoRoT mission, pre-launch status, stellar seismology and planet finding, eds. M. Fridlund, A. Baglin, J. Lochard, & L. Conroy, ESA SP-1306 (Noordwijk, The Netherlands: ESA Publication Division)

Barklem, P. S., Stempels, H. C., Allende Prieto, C., et al. 2002, A&A, 385, 951
Bessel, M.S., Castelli, F., & Plez, B. 1998, A&A, 333, 231
Breger, M. 1972, ApJ, 171, 539
Breger, M. 1993, A&A, 271, 482
Breger, M., & Pamyatnykh, A. A. 1998, A&A, 332, 958
Breger, M., Lenz, P., & Pamyatnykh, A. A. 2008, CoAst, 157, 56
Breger, M., Lenz, P., & Pamyatnykh, A. A. 2009, MNRAS, 396, 291
Breger, M., Balona, L., Lenz, P., et al. 2011, MNRAS, 414, 1721
Bouabid, M.-P., Montalbán, J., Miglio, A., et al. 2001, A&A, 531, 145
Carroll, J. A. 1933a, MNRAS, 93, 478
Carroll, J. A. 1933b, MNRAS, 93, 680
Casey, M., Zwintz, K., Guenther, D. B., et al. 2013, MNRAS, 428, 2596
Cutri, R. M., Wright, E. L., Conrow, T., et al. 2012, VizieR On-line Data Catalog: II/311
Demarque, P., Guenther, D. B., Li, L. H., Mazumdar, A., & Straka, C. W. 2008, Ap&SS, 316, 31
Donati, J.-F., Semel, M., Carter, B. D., Rees, D. E., & Collier Cameron, A. 1997, MNRAS, 291, 658
Dravins, D., Lindegren, L., & Torkelsson, U. 1990, A&A, 237, 137
Fossati, L., Bagnulo, S., Monier, R., et al. 2007, A&A, 476, 911
Fossati, L., Ryabchikova, T., Bagnulo, S., et al. 2009, A&A, 503, 945
Fossati, L, Folsom, C. P., Bagnulo, S., et al. 2011a, MNRAS, 413, 1132
Fossati, L., Ryabchikova, T., Shulyak, D. V., et al. 2011b, MNRAS, 417, 495
Glazunova, L. V., Yushchenko, A. V., Tsymbal, V. V., et al. 2008, AJ, 136, 1736
Guenther, D. B. 1994, ApJ, 422, 400
Guenther, D. B., & Brown, K. I. T. 2004, ApJ, 600, 419
Guenther, D. B., Kallinger, T., Zwintz, K., et al. 2009, ApJ, 704, 1710
Hareter, M., Reegen, P., Kuschnig, R., et al. 2008, CoAst, 156, 48
Hog, E., Fabricius, C., Makarov, V. V., et al. 2000, A&A, 355, 27
Kallinger, T., Reegen, P., & Weiss, W. W. 2008, A&A, 481, 571
Kharchenko, N. V. 2001, Kinemat. Phys. Celest. Bodies, 17, 409
Kharchenko, N. N., Piskunov, A. E., Roeser, S., Schilback, E., & Scholz, R. D. 2005, A&A, 438, 1163
Kochukhov, O. 2007, in Physics of Magnetic Stars, eds. I. I. Romanyuk, D. O. Kudryavtsev, O. M. Neizvestnaya, & V. M. Shapoval, Proc. Int. Conf. Special Astrophysical Observatory, RAS, 109
Kochukhov, O., Makaganiuk, V., & Piskunov, N. 2010, A&A, 524, A5
Kupka, F., Piskunov, N., Ryabchikova, T. A., Stempels, H. C., & Weiss, W. W. 1999, A&AS, 138, 119
Kurucz, R. 1993, ATLAS9: Stellar Atmosphere Programs and 2 km s^{-1} grid, Kurucz CD-ROM No. 13 (Cambridge: Smithsonian Astrophysical Observatory)
Kuschnig, R., Weiss, W. W., Gruber, R., Bely, P. Y., & Jenkner, H. 1997, A&A, 328, 544
Lenz, P., & Breger, M. 2005, CoAst, 146, 53

Lynga, G. 1987, Catalogue of Open Cluster Data, 5th edn. (Lund Observatory, Sweden)
Marconi, M., & Palla, F. 1998, AJ, 507, L141
Mashonkina, L., Gehren, T., Shi, J.-R., Korn, A. J., & Grupp, F. 2011, A&A, 528, 87
Mermilliod, J.-C., & Mermilliod, M. 1994, in Catalogue of Mean UBV Data on Stars, VI (New York: Springer-Verlag), 1387
Moon, T. T., & Dworetsky, M. M. 1985, MNRAS, 217, 305
Piskunov, N. E., Kupka, F., Ryabchikova, T. A., Weiss, W. W., & Jeffery, C. S. 1995, A&AS, 112, 525
Reegen, P. 2007, A&A, 467, 135
Reegen, P., Kallinger, T., Frast, D., et al. 2006, MNRAS, 367, 1417
Reiners, A., & Schmitt, J. H. M. M. 2002a, A&A, 384, 155
Reiners, A., & Schmitt, J. H. M. M. 2002b, A&A, 393, L77
Ripepi, V., Bernabei, S., Marconi, M., et al. 2006, A&A, 449, 335
Ripepi, V., Cusano, F., di Criscienzo, M., et al. 2011, MNRAS, 416, 1535
Ryabchikova, T. A., Piskunov, N. E., Stempels, H. C., Kupka, F., & Weiss, W. W. 1999, Phis. Scr., T83, 162
Sagar, R., Piskunov, A. E., Miakutin, V. I., & Joshi, U. C. 1986, MNRAS, 220, 383
Shulyak, D., Tsymbal, V., Ryabchikova, T., Stütz Ch., & Weiss, W. W. 2004, A&A, 428, 993
Skiff, B. A. 2005, General Catalog of Stellar Spectral Classifications (Lowell Observatory)
Sung, H., Bessel, M. S., & Lee, S.-W. 1997, AJ, 114, 2644
Sung, H., Bessel, M. S., & Chun, M.Y. 2004, AJ, 128, 1684
Sung, H., Sauffer, J. R., & Bessel, M. S. 2009, AJ, 138, 1116
Tsymbal, V. V. 1996, in Model Atmospheres and Spectral Synthesis, eds. S. J. Adelman, F. Kupka, & W. W. Weiss, ASP Conf. Ser., 108, 198
van der Bliek, N. S., Manfroid, J., & Bouchet, P. 1996, A&AS, 119, 547
Van Hamme, W. 1993, AJ, 106, 20
Walker, G., Matthews, J. M., Kuschnig, R., et al. 2003, PASP, 115, 1023
Weiss, W. 2006, in Proc. The CoRoT Mission Pre Launch Status, Stellar Seismology and Planet Finding, eds. M. Fridlund, A. Baglin, J. Lochard, & L. Conroy (Noordwijk, The Netherlands: ESA Publications Division), ESA SP 1306, 93
Weisskopf, M. C., Brinkman, B., Canizares, S., et al. 2002, PASP, 114, 1
Werner, M. W., Roellig, T. L., Low, F. J., et al. 2004, ApJS, 154, 1
Wright, E. L., Eisenhardt, P. R. M., Mainzer, A. K., et al. 2010, AJ, 140, 1868
Zacharias, N., Monet, D. G., Levine, S. E., et al. 2005, BAAS, 36, 1418
Zwintz, K. 2008, ApJ, 673, 1088
Zwintz, K., Hareter, M., Kuschnig, R., et al. 2009, A&A, 502, 239
Zwintz, K., Kallinger T., Guenther, D. B., et al. 2011a, ApJ, 729, 20
Zwintz, K., Lenz, P., Breger, M., et al. 2011b, A&A, 533, A133
Zwintz, K., Fossati, L., Ryabchikova, T. A., et al. 2013, A&A, 550, A121